Surface photovoltaic effect and electronic structure of β-InSe

L. Kang,[1] L. Shen [ORCID],[1] Y. J. Chen,[1] S. C. Sun,[1] X. Gu,[1] H. J. Zheng,[2] Z. K. Liu,[2,3] J. X. Wu,[4] H. L. Peng,[4] F. W. Zheng,[5] P. Zhang,[5] L. X. Yang [ORCID],[1,6,*] and Y. L. Chen[1,2,3,7,†]

[1]*State Key Laboratory of Low Dimensional Quantum Physics, Department of Physics, Tsinghua University, Beijing 100084, China*
[2]*School of Physical Science and Technology, ShanghaiTech University and CAS-Shanghai Science Research Center, Shanghai 201210, China*
[3]*ShanghaiTech Laboratory for Topological Physics, Shanghai 200031, China*
[4]*Center for Nanochemistry, Beijing Science and Engineering Centre for Nanocarbons, College of Chemistry and Molecular Engineering, Peking University, Beijing 100871, China*
[5]*Institute of Applied Physics and Computational Mathematics, Beijing 100088, China*
[6]*Frontier Science Center for Quantum Information, Beijing 100084, China*
[7]*Department of Physics, Clarendon Laboratory, University of Oxford, Parks Road, Oxford OX1 3PU, United Kingdom*

Using high-resolution angle-resolved photoemission spectroscopy, we systematically investigate the electronic structure of β-InSe, a van der Waals semiconductor with a direct band gap. Our measurements show a good agreement with *ab initio* calculations, which helps reveal the important impact of spin-orbit coupling on the electronic structure of β-InSe. Using surface potassium doping, we tune the chemical potential of the system and observe the unoccupied conduction band. The direct band gap is determined to be about 1.3 eV. Interestingly, we observe a global band shift when the sample is illuminated by a continuous-wave laser at 632.8 nm, which can be understood by an efficient surface photovoltaic effect. The surface photovoltaic can be tuned by *in situ* surface potassium doping. Our results not only provide important insights into the semiconducting properties of InSe, but also suggest a feasible method to study and engineer the surface photovoltaic effect in InSe-based devices.

I. INTRODUCTION

van der Waals compounds represent a large variety of layered materials with extremely weak interlayer interaction. They exhibit various intriguing properties that not only provide important scientific implications in condensed-matter physics but also promise broad application potentials in the electronic devices [1–11]. As a prime example, van der Waals semiconductor InSe has attracted particular research attention due to its extraordinary properties in optoelectronics, photovoltaics, nonlinear optics, and thermoelectrics [1,12–15]. Its carrier mobility can reach as high as $1000 \, \text{cm}^2/\text{V} \cdot \text{s}$ at room temperature and $>10\,000 \, \text{cm}^2/\text{V} \cdot \text{s}$ at liquid-helium temperature [1,16,17]; its band gap and work function can be effectively tuned by changing the crystal thickness [18–20]; the strong spin-orbit coupling (SOC) of few-layer InSe can likewise be controlled by electrostatic gating method [21]. For practical applications, InSe films are considered as electrode material for lithium-ion battery and potential energy conversion units [22–27].

There are three types of layered InSe polymorphs (β, γ, and ε) that differ from each other by the stacking order of primitive InSe layers [28,29]. In order to understand and engineer their extraordinary properties, it is instructive to systematically study their electronic structures. Although their basic electronic structures have been theoretically and experimentally investigated [20,30–37], direct determination of the crucial semiconducting gap in different InSe crystals is still in demand [18,31,36]. Moreover, it is important to study the response of the electronic structure to the external photoexcitation, in order to understand and improve the photovoltaic properties of InSe-based electronic devices.

In this paper, we systematically investigate the electronic structure of β-InSe using high-resolution angle-resolved photoemission spectroscopy (ARPES). By comparing with *ab initio* calculations, we recognize important impact of the strong SOC on the electronic structure of β-InSe: it lifts the band degeneracy at high-symmetry points of the Brillouin zone (BZ). We also note that a nodal line along *AL* survives the strong SOC due to the protection by the nonsymmorphic crystal symmetry of β-InSe. By surface potassium doping, we tune the chemical potential of β-InSe, observe the unoccupied conduction bands, and directly determine that the semiconducting band gap is about 1.3 eV. Interestingly, we observe an upward shift of the whole band structure together with the increase of ARPES cutoff energy when the sample is illuminated by a continuous-wave (cw) laser at 632.8 nm, indicating an efficient surface photovoltaic (SPV) effect in β-InSe [22] that can be tuned by surface potassium doping. Our results provide important insights into the electronic properties of β-InSe and its response to visible light, which will shed light on the design of InSe-based electronic and solar-energy devices for different applications.

_____
*lxyang@tsinghua.edu.cn
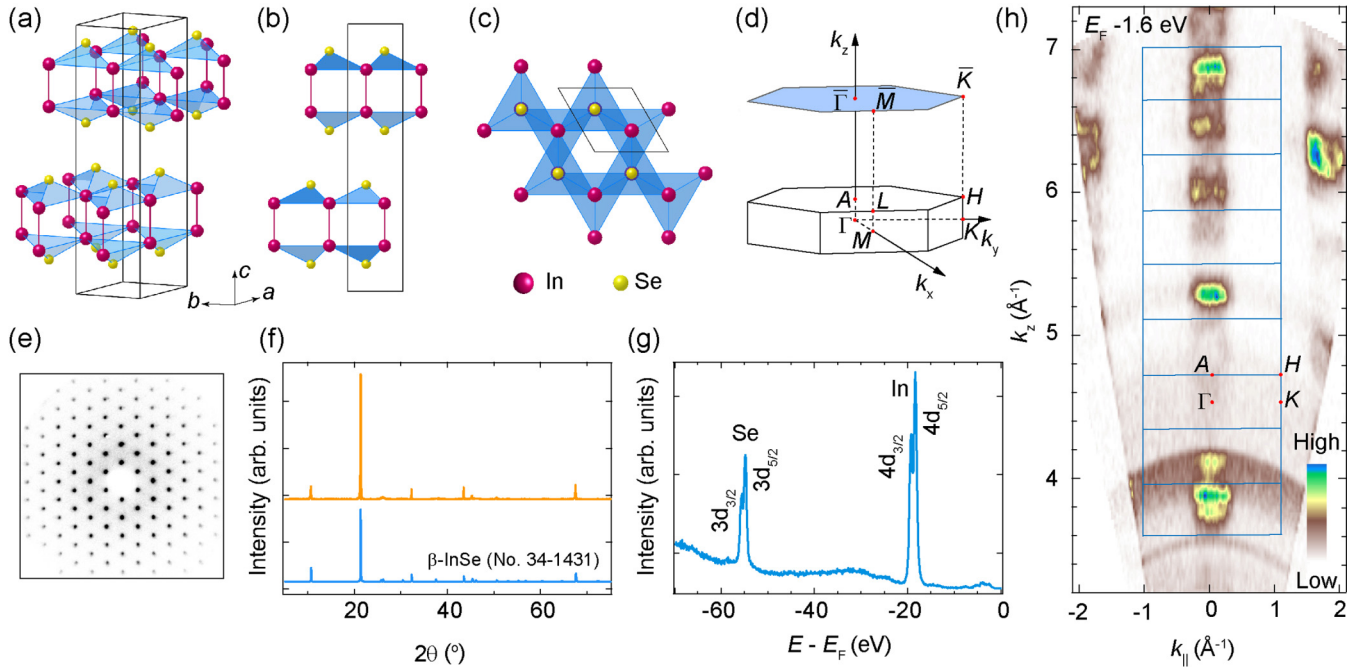†yulin.chen@physics.ox.ac.uk

FIG. 1. Characterization of bulk β-InSe crystals. (a) Schematic illustration of the lattice structure of β-InSe. (b) Side view and (c) top view of the crystal structure. The purple and yellow spheres refer to indium (In) and selenium (Se) atoms, respectively. (d) The Brillouin zone of bulk β-InSe and its (001) surface projection with high-symmetry points marked. (e) Electron diffraction spectrum of β-InSe crystal. (f) X-ray powder-diffraction spectrum of our β-InSe crystal (yellow curve) and standard x-ray diffraction spectrum (blue curve). (g) Core-level photoemission spectrum of InSe, showing characteristic In and Se peaks. (h) The constant-energy contours at 1.6 eV below the Fermi energy (E_F) in the $k_{||}$-k_z plane. Data were collected using linear-horizontally (LH) polarized photons ranging from 44 to 230 eV at 6 K.

II. METHOD

High-quality β-InSe single crystals were prepared via a modified Bridgman method. The stoichiometric high-purity In powder (99.999%) and Se powder (99.999%) were mechanically mixed together first, then loaded into a quartz tube which was pumped into vacuum (10^{-1} Pa) to exclude the oxygen. The evacuated quartz tube was then inserted in a horizontal single heating-zone furnace. The temperature gradient was naturally generated between the center and the edge of the furnace. The temperature was gradually raised up to 1223 K within 2 h and kept for 1 h to form a completely molten and uniform In-Se mixture. Then the mixture was slowly cooled down to 573 K for 24 h, followed by natural cooling to room temperature to form bulk crystals. No post annealing was conducted on the samples for ARPES measurements.

ARPES measurements were performed at beamline I05 of Diamond Light Source (DLS) and beamline 13U of National Synchrotron Radiation Laboratory (NSRL). The samples were *in situ* cleaved along the (001) direction under ultrahigh vacuum below 1.5×10^{-10} Torr. Data were collected by Scienta R4000 analyzers at DLS and NSRL with overall energy and angle resolutions of 20 meV and 0.2°, respectively. ARPES measurements after surface doping and under laser illumination were performed using a helium discharge lamp and DA30L analyzer in Tsinghua University, Beijing, China and ShanghaiTech University, Shanghai, China. The surface doping was operated *in situ* at 65 K by evaporating

potassium atoms using an SAES alkali-metal source after well outgassing. Density-functional theory (DFT) calculations were performed using the Vienna *Ab initio* Simulation Package (VASP) [38,39].

III. RESULTS AND DISCUSSION

β-InSe belongs to the $P6_3/mmc$ space group (No. 194). It exhibits a layered structure with van der Waals stacking of InSe layers. In each unit cell, there are two InSe layers that relatively rotate 180° about the c axis and shift by a vector of (a/2, b/2, c/2), which respects the glide symmetry [Figs. 1(a)–1(c)]. Each InSe layer consists of four atomic layers of Se-In-In-Se and forms a honeycomb structure with in-plane lattice parameters $a = b = 4.05$ Å [Figs. 1(a)–1(c)]. Figure 1(d) shows the three-dimensional (3D) BZ and its surface projection with high-symmetry points indicated.

The crystal structure of the samples used in this work has been characterized by electron diffraction and x-ray powder diffraction measurements [Figs. 1(e) and 1(f)], showing the high quality of the samples. The core-level photoemission spectrum in Fig. 1(g) shows sharp peaks from In and Se elements. The photon energy-dependent measurement in Fig. 1(h) shows a clear periodic variation of ARPES intensity near the 1.6 eV below the Fermi energy (E_F), despite the van der Waals interlayer coupling in InSe (see Supplemental Material, Fig. S2 [40]). From the $k_{||}$-k_z map in Fig. 1(h), we
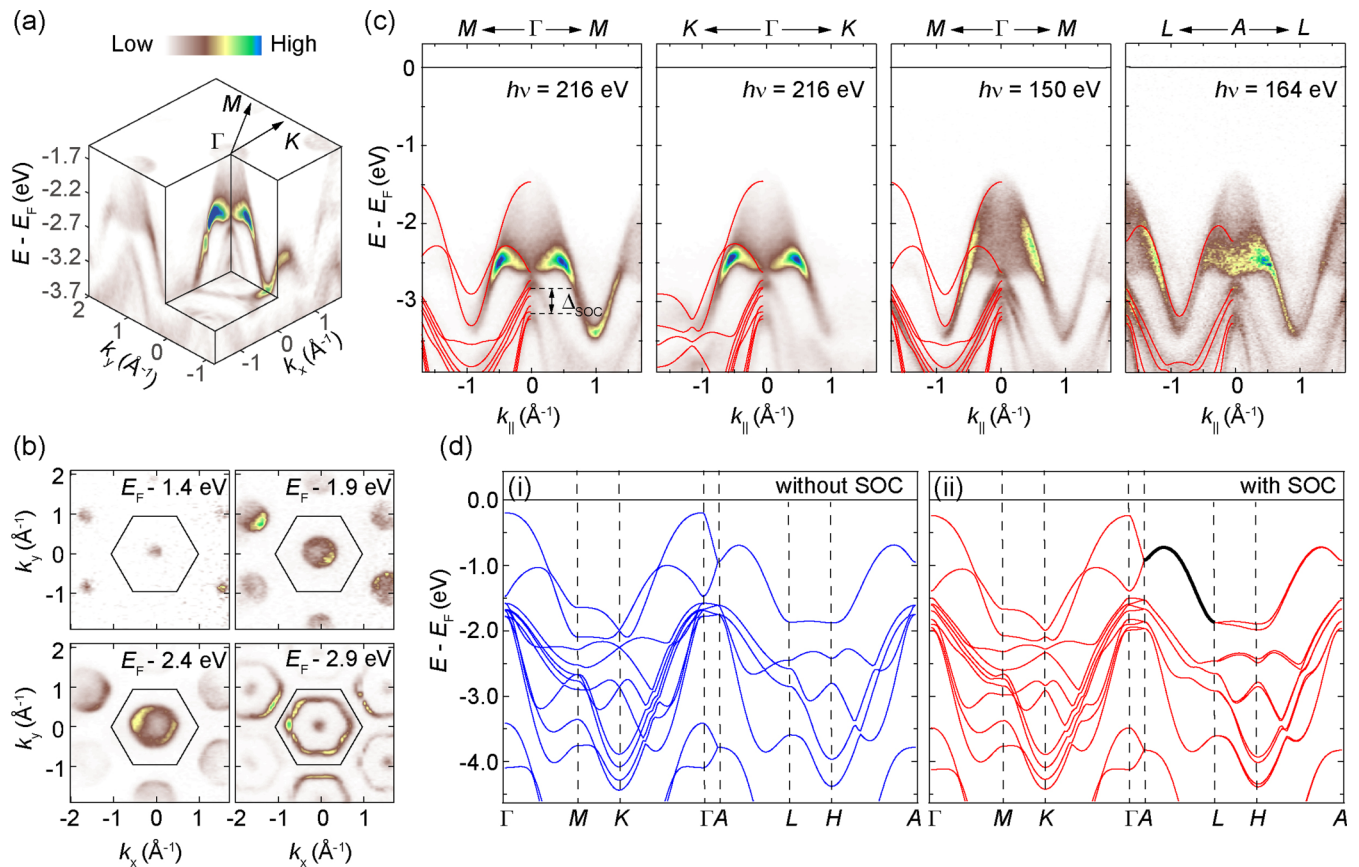
FIG. 2. Electronic structure of pristine β-InSe. (a) Three-dimensional plot of the electronic structure of β-InSe. (b) Constant-energy contours in the ΓMK plane at selected binding energies. Each contour is integrated in an energy window of 20 meV. Data in panels (a) and (b) were collected with LH photons of 216 eV at 6 K. (c) Band dispersions along high-symmetry directions with corresponding calculated result overlaid. (d) Calculated band structure of β-InSe without (i) and with (ii) SOC. The calculated result overlaid in panel (c) is shifted in energy direction to match the experiment.

can determine the photon energies that reach the *AHL* and ΓKM planes in the 3D BZ.

Figure 2 shows the basic electronic structure of β-InSe. Figures 2(a) and 2(b) show the 3D plots of ARPES spectra and constant-energy contours at selected binding energies. With increasing binding energy, the constant-energy contours gradually evolve from a pointlike feature into a hexagon around the Γ point, consistent with the hexagonal crystal structure [Fig. 2(b)]. Figure 2(c) shows the band dispersions along high-symmetry directions. The calculated band dispersions are overlaid on the experimental data for the comparison. Note that due to the limited k_z resolution, the spectra at Γ and A mix in the measurements with different photon energies. We observe a good agreement between our experimental and *ab initio* calculated results with SOC included [Fig. 2(d)]. The SOC modifies the electronic structure of β-InSe by inducing a band gap (Δ_{SOC}) of about 0.33 eV near -3 eV along ΓA, which is observed by ARPES measurements in Fig. 2(c). It is worth noting that there exists a nodal line along *AL* that is protected by the nonsymmorphic crystal symmetry [41], as indicated by the thick black line in the band calculation [Fig. 2(d)(ii)]. Previous studies suggest that different stacking sequence of InSe layers changes the k_z dispersion, the num-

ber of energy bands, and the band-gap size in different InSe polymorphs [18–20,30–32,42]. However, due to the limited k_z resolution in ARPES measurement, it is challenging to resolve these subtle differences.

In order to determine the magnitude of the semiconducting gap, we use surface potassium doping to raise the chemical potential and detect the conduction bands. After doping 0.16 monolayer (ML) of potassium atoms on the sample surface [43], a small electron pocket emerges in the Fermi surface, while the constant-energy contours from the valence bands barely change [Fig. 3(a)]. From the band dispersions along ΓM [Fig. 3(b)], we can observe the conduction bands and determine the direct band gap is 1.3 ± 0.1 eV, consistent with previous experimental and calculated results [19,20,30–32,42]. The band gap is also measured using 21.2 eV (near Γ) photons delivered by discharge helium lamp. As shown in Figs. 3(b) and 3(c), the band gap can be accurately determined from the edges of the energy distribution curve (EDC) peaks, which is in good consistency with the value measured using synchrotron-based ARPES in Fig. 3(a). More results about the evolution of the band structure with surface potassium doping can be found in the Supplemental Material [40].
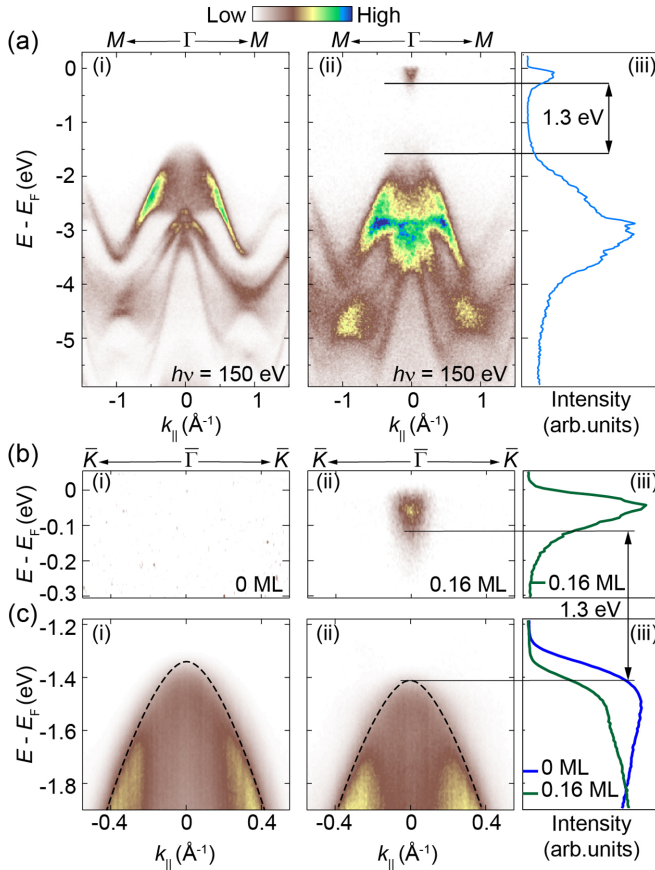
FIG. 3. Evaluation of the band gap of β-InSe. (a) Band dispersions along the ΓM direction before (i) and after (ii) potassium doping. The band gap is determined to be 1.3 ± 0.1 eV, consistent with the EDC at Γ (iii). Data in panel (a) were measured at 6 K. (b), (c) Band dispersion near E_F (b) and the valence band (c) before (i) and after (ii) surface potassium doping. The panels (b)(iii) and (c)(iii) show the corresponding EDCs at Γ. The black arrows indicate the band gap. The black dashed lines in (c) are guides to the eyes for the valence band. ARPES intensity in panel (b)(ii) is timed by 40 to use the same intensity color scale as in panels (a) and (c).

InSe is well known for its extraordinary optoelectronic and photovoltaic properties [1,12,14,22]. In Fig. 4, in order to investigate the response of the electronic structure of β-InSe to the photoexcitation, we measure its band structure while illuminating the sample surface with a cw He-Ne laser (center wavelength at 632.8 nm). The average laser power is about 2 mW with a power stability of $\pm 2\%$. The spot size is slightly larger than the sample (typically 1×1 mm^2). No clear heating effect was observed during this measurement. For both the pristine [Fig. 4(a)] and potassium-doped β-InSe [Figs. 4(b) and 4(c)], we observe global band shift towards low binding energies when the sample is illuminated by laser, which is reversible when the laser is turned off. Moreover, the cutoff energy of the ARPES spectra showing the conduction bands after surface potassium doping is raised by about 42 meV when the sample is illuminated [Fig. 4(b)(ii)]. We argue that

the photoillumination induces unbalanced chemical potentials of the sample surface and bulk, creates an effective electric field on the sample surface, and raises the cutoff energy of photoelectrons, which can be understood by the SPV effect, as schematically shown in Fig. 4(d). Without laser illumination, the semiconducting InSe shows a downward band bending [Fig. 4(e)]. The illuminated laser photons create electron-hole pairs across the band gap. The excited electrons and holes move towards opposite directions due to the field existing in the band-bending region [Fig. 4(f)]. The transfer of carriers flattens the band bending and establishes an effective electrostatic potential on the sample surface [44], thus increasing the kinetic energy of the photoelectrons. Since the balance between the chemical potentials of the sample surface and bulk takes place on a timescale less than 10 ns [45–47], the surface photovoltaic effect will disappear once the laser is turned off.

Interestingly, the shift of the valence-band top increases from about 30 meV in the pristine sample to about 42 meV in potassium-doped sample, suggesting that the SPV effect can be effectively tuned by surface potassium doping, similar to the SPV effect in the semiconductor WSe$_2$ [48]. Through surface potassium doping, the Fermi level, work function, semiconducting gap, and surface electric field can be optimized for the SPV effect [42], which opens a window to improve the SPV efficiency of InSe-based functional devices. On the other hand, our results suggest that ARPES measurement under photoillumination is a feasible noncontacting tool to study the SPV effect, in contrast to previous SPV experiment with electrodes contacting the devices [22].

IV. CONCLUSION

In conclusion, we have presented a comprehensive study of the electronic structure of bulk β-InSe by ARPES experiment and *ab initio* calculation. We observe clear k_z dispersion despite the weak van der Waals interlayer coupling in the crystals. Using surface-doping method, we successfully observe the unoccupied conduction bands and determine the direct band gap of β-InSe. We show a feasible method to directly observe and control the SPV effect with ARPES measurement. Our work provides important insights into the understanding and application of intriguing properties of β-InSe.
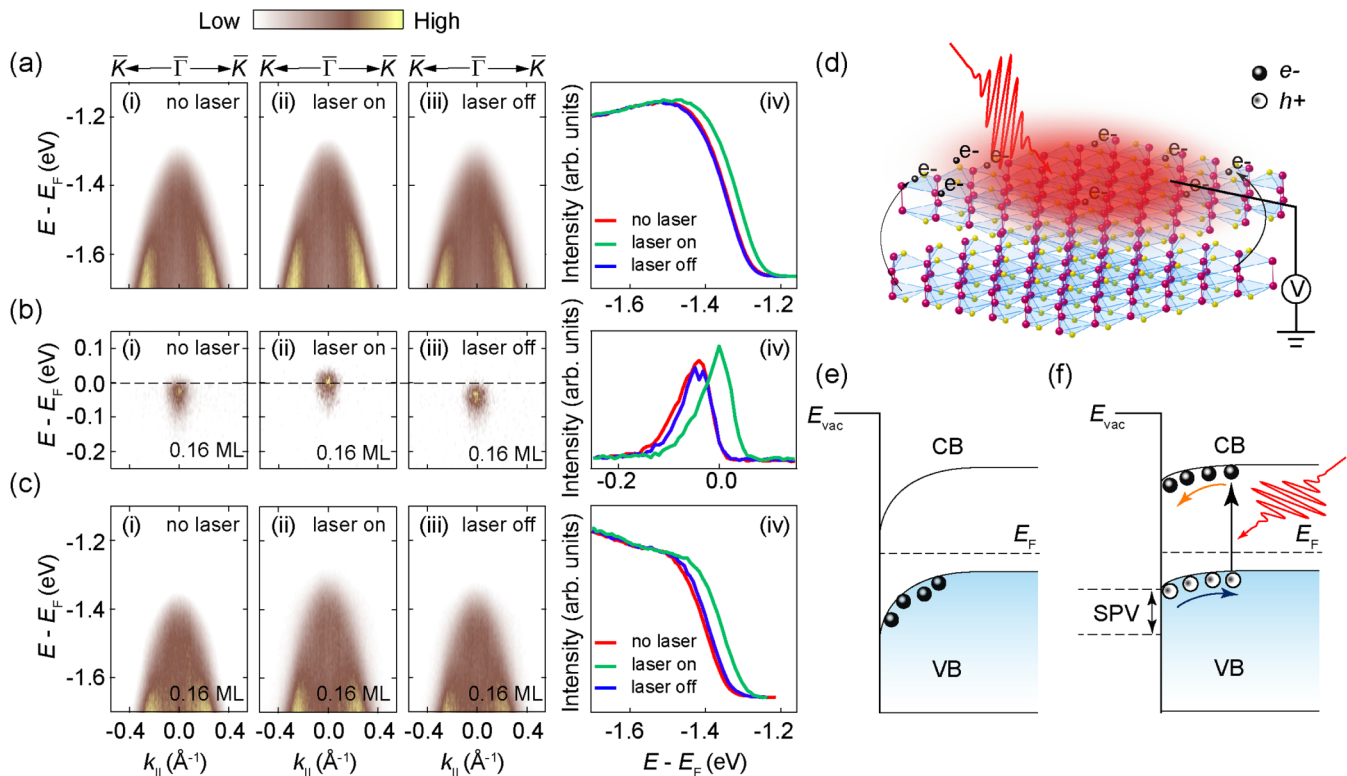
FIG. 4. Surface photovoltaic effect of β-InSe. (a) Valence-band structure measured with and without laser illumination on the pristine crystals. (b) Conduction- and (c) valence bands measured with and without laser illumination after surface potassium doping of 0.16 ML. The slight difference between the spectra before and after laser illumination may be due to the laser-induced desorption of potassium atoms. (d) Schematic illustration of the SPV effect on β-InSe. The photoillumination creates an effective electric field on the sample surface. (e) Band bending in β-InSe. (f) Flattening of the band bending due to the laser illumination.

[1] D. A. Bandurin, A. V. Tyurnina, G. L. Yu, A. Mishchenko, V. Zólyomi, S. V. Morozov, R. K. Kumar, R. V. Gorbachev, Z. R. Kudrynskyi, S. Pezzini, Z. D. Kovalyuk, U. Zeitler, K. S. Novoselov, A. Patanè, L. Eaves, I. V. Grigorieva, V. I. Fal'ko, A. K. Geim, and Y. Cao, Nat. Nanotechnol. **12**, 223 (2017).

[2] K. S. Novoselov, A. Mishchenko, A. Carvalho, and A. H. Castro Neto, Science **353**, aac9439 (2016).

[3] P. Ajayan, P. Kim, and K. Banerjee, Phys. Today **69**(9), 38 (2016).

[4] D. N. Basov, M. M. Fogler, and F. J. García de Abajo, Science **354**, aag1992 (2016).

[5] K. S. Burch, D. Mandrus, and J.-G. Park, Nature (London) **563**, 47 (2018).

[6] S. Das, J. A. Robinson, M. Dubey, H. Terrones, and M. Terrones, Annu. Rev. Mater. Res. **45**, 1 (2015).

[7] Y. Deng, Y. Yu, M. Z. Shi, Z. Guo, Z. Xu, J. Wang, X. H. Chen, and Y. Zhang, Science **367**, 895 (2020).

[8] Y. Deng, Y. Yu, Y. Song, J. Zhang, N. Z. Wang, Z. Sun, Y. Yi, Y. Z. Wu, S. Wu, J. Zhu, J. Wang, X. H. Chen, and Y. Zhang, Nature (London) **563**, 94 (2018).

[9] W. Ding, J. Zhu, Z. Wang, Y. Gao, D. Xiao, Y. Gu, Z. Zhang, and W. Zhu, Nat. Commun. **8**, 14956 (2017).

[10] Y. Liu, N. O. Weiss, X. Duan, H.-C. Cheng, Y. Huang, and X. Duan, Nat. Rev. Mater. **1**, 16042 (2016).

[11] X. Xu, W. Yao, D. Xiao, and T. F. Heinz, Nat. Phys. **10**, 343 (2014).

[12] Z. Chen, J. Biscaras, and A. Shukla, Nanoscale **7**, 5981 (2015).

[13] G. Han, Z.-G. Chen, J. Drennan, and J. Zou, Small **10**, 2747 (2014).

[14] A. Segura, J. P. Guesdon, J. M. Besson, and A. Chevy, J. Appl. Phys. **54**, 876 (1983).

[15] R. Kaindl, F. Eickemeyer, M. Woerner, and T. Elsaesser, Appl. Phys. Lett. **75**, 1060 (1999).

[16] C. Sun, H. Xiang, B. Xu, Y. Xia, J. Yin, and Z. Liu, Appl. Phys. Express **9**, 035203 (2016).

[17] A. Segura, F. Pomer, A. Cantarero, W. Krause, and A. Chevy, Phys. Rev. B **29**, 5708 (1984).

[18] G. W. Mudd, S. A. Svatek, T. Ren, A. Patane, O. Makarovsky, L. Eaves, P. H. Beton, Z. D. Kovalyuk, G. V. Lashkarev, Z. R. Kudrynskyi, and A. I. Dmitriev, Adv. Mater. **25**, 5714 (2013).

[19] Y. Guo and J. Robertson, Phys. Rev. Mater. **1**, 044004 (2017).

[20] M. J. Hamer, J. Zultak, A. V. Tyurnina, V. Zólyomi, D. Terry, A. Barinov, A. Garner, J. Donoghue, A. P. Rooney, V. Kandyba, A. Giampietri, A. Graham, N. Teutsch, X. Xia, M. Koperski, S. J. Haigh, V. I. Fal'ko, R. V. Gorbachev, and N. R. Wilson, ACS Nano **13**, 2136 (2019).

[21] K. Premasiri, S. Kumar, S. Sucharitakul, U. Kumar, R. Sankar, F. Chou, Y.-T. Chen, and X. Gao, Nano Lett. **18**, 4403 (2018).

[22] C.-H. Ho and Y.-J. Chu, Adv. Opt. Mater. **3**, 1750 (2015).

[23] J. Martínez-Pastor, A. Segura, J. L. Valdés, and A. Chevy, J. Appl. Phys. **62**, 1477 (1987).

[24] J. F. Sánchez-Royo, A. Segura, O. Lang, C. Pettenkofer, W. Jaegermann, A. Chevy, and L. Roa, Thin Solid Films **307**, 283 (1997).

[25] J. F. Sánchez-Royo, A. Segura, O. Lang, E. Schaar, C. Pettenkofer, W. Jaegermann, L. Roa, and A. Chevy, J. Appl. Phys. **90**, 2818 (2001).

[26] M. Brotons-Gisbert, D. Andres-Penares, J. Suh, F. Hidalgo, R. Abargues, P. J. Rodríguez-Cantó, A. Segura, A. Cros, G. Tobias, E. Canadell, P. Ordejón, J. Wu, J. P. Martínez-Pastor, and J. F. Sánchez-Royo, Nano Lett. **16**, 3221 (2016).

[27] C. Julien and M. Balkanski, Appl. Surf. Sci. **48–49**, 1 (1991).

[28] A. M. Mancini, G. Micocci, and A. Rizzo, Mater. Chem. Phys. **9**, 29 (1983).

[29] T. Ikari, S. Shigetomi, and K. Hashimoto, Phys. Status Solidi B **111**, 477 (1982).

[30] D. W. Boukhvalov, B. Gurbulak, S. Duman, L. Wang, A. Politano, L. S. Caputi, G. Chiarello, and A. Cupolillo, Nanomaterials (Basel) **7**, 372 (2017).

[31] H. Henck, D. Pierucci, J. Zribi, F. Bisti, E. Papalazarou, J.-C. Girard, J. Chaste, F. Bertran, P. Le Fèvre, F. Sirotti, L. Perfetti, C. Giorgetti, A. Shukla, J. E. Rault, and A. Ouerghi, Phys. Rev. Mater. **3**, 034004 (2019).

[32] A. Politano, D. Campi, M. Cattelan, I. Ben Amara, S. Jaziri, A. Mazzotti, A. Barinov, B. Gürbulak, S. Duman, S. Agnoli, L. S. Caputi, G. Granozzi, and A. Cupolillo, Sci. Rep. **7**, 3445 (2017).

[33] A. Amokrane, F. Proix, S. Monkad, A. Cricenti, C. Barchesi, M. Eddrief, K. Amimer, and C. Sébenne, J. Phys.: Condens. Matter **11**, 4303 (1999).

[34] P. Larsen and S. Chiang, Phys. Rev. B **15**, 3200 (1977).

[35] I. A. Kibirev, A. V. Matetskiy, A. V. Zotov, and A. A. Saranin, Appl. Phys. Lett. **112**, 191602 (2018).

[36] D. K. Sang, H. Wang, M. Qiu, R. Cao, Z. Guo, J. Zhao, Y. Li, Q. Xiao, D. Fan, and H. Zhang, Nanomaterials **9**, 82 (2019).

[37] H. Xu, W. Wang, Y. Zhao, X. Zhang, Y. Feng, J. Tu, C. Gu, Y. Sun, C. Liu, Y. Nie, I. C. Edmond Turcu, Y. Xu, and L. He, AIP Adv. **8**, 055123 (2018).

[38] P. E. Blöchl, Phys. Rev. B **50**, 17953 (1994).

[39] J. P. Perdew, K. Burke, and M. Ernzerhof, Phys. Rev. Lett. **77**, 3865 (1996).

[40] See Supplemental Material at http://link.aps.org/supplemental/ 10.1103/PhysRevMaterials.4.124604 for (I) Charging test. (II) k_z dispersion of β-InSe. (III) Conduction band in the calculation. (IV) Evolution of the band structure of InSe with *in situ* surface potassium doping. (V) Observation of additional states near the valence-band top.

[41] X. Xu, J. Jiang, W. J. Shi, V. Süß, C. Shekhar, S. C. Sun, Y. J. Chen, S. K. Mo, C. Felser, B. H. Yan, H. F. Yang, Z. K. Liu, Y. Sun, L. X. Yang, and Y. L. Chen, Phys. Rev. B **99**, 195106 (2019).

[42] Z. Zhang, Z. Chen, M. Bouaziz, C. Giorgetti, H. Yi, J. Avila, B. Tian, A. Shukla, L. Perfetti, D. Fan, Y. Li, and A. Bendounan, ACS Nano **13**, 13486 (2019).

[43] H. F. Yang, L. X. Yang, Z. K. Liu, Y. Sun, C. Chen, H. Peng, M. Schmidt, D. Prabhakaran, B. A. Bernevig, C. Felser, B. H. Yan, and Y. L. Chen, Nat. Commun. **10**, 3478 (2019).

[44] Z. Zhang and J. T. Yates, Chem. Rev. **112**, 5520 (2012).

[45] L. X. Yang, G. Rohde, T. Rohwer, A. Stange, K. Hanff, C. Sohrt, L. Rettig, R. Cortés, F. Chen, D. L. Feng, T. Wolf, B. Kamble, I. Eremin, T. Popmintchev, M. M. Murnane, H. C. Kapteyn, L. Kipp, J. Fink, M. Bauer, U. Bovensiepen, and K. Rossnagel, Phys. Rev. Lett. **112**, 207001 (2014).

[46] C. Zhong, V. K. Sangwan, J. Kang, J. Luxa, Z. Sofer, M. C. Hersam, and E. A. Weiss, J. Phys. Chem. Lett. **10**, 493 (2019).

[47] R. Wang, X. Jiang, S. Gao, J. Zhao, F. Zhang, W. Huang, T. Fan, W. Liang, Z. Li, H. Huang, Z. Guo, H. Wang, Y. Zhang, X. Zhang, Z. Luo, and H. Zhang, Adv. Mater. Interfaces **6**, 1900171 (2019).

[48] J. Buck, J. Iwicki, K. Rossnagel, and L. Kipp, Phys. Rev. B **83**, 075312 (2011).